LIMNOLOGY and OCEANOGRAPHY



Elmnol. Oceanogr. 67, 2022, 2174–2189
© 2022 Association for the Sciences of Limnology and Oceanography.
doi: 10.1002/lno.12196

Seasonal hypoxia and temperature inversions in a tropical bay

Anne E. Adelson ⁰, ^{1*} Andrew H. Altieri ⁰, ^{2,3} Ximena Boza ⁰, ³ Rachel Collin ⁰, ³ Kristen A. Davis ⁰, ^{4,5} Alan Gaul ⁰, ⁶ Sarah N. Giddings ⁰, ¹ Victoria Reed, ³ Geno Pawlak ⁰, ^{1,6}

¹Scripps Institution of Oceanography, University of California, San Diego, La Jolla, California

²Department of Environmental Engineering Sciences, Engineering School of Sustainable Infrastructure and Environment, University of Florida, Gainesville, Florida

³Smithsonian Tropical Research Institute, Balboa Ancon, Panama

⁴Department of Civil and Environmental Engineering, University of California, Irvine, Irvine, California

⁵Department of Earth System Science, University of California, Irvine, Irvine, California

⁶Department of Mechanical and Aerospace Engineering, University of California, San Diego, La Jolla, California

Abstract

Dissolved oxygen (DO) is a critically important ecological variable, and the prevalence of marine hypoxia is expected to increase due to the combined effects of ocean warming and eutrophication. Thermal stress can co-occur with hypoxia, especially in tropical systems, and can exacerbate its effects. We examine the physical processes that are important in regulating hypoxia and temperature inversions in Bahía Almirante, a semi-enclosed tropical embayment on the Caribbean coast of Panama. A 10-yr record of observations at 7 locations within Bahía Almirante reveals seasonal temperature inversions and hypoxia at depth that often co-occur. These features are more severe and persistent in the back bay, though they occur throughout Bahía Almirante. DO reductions correspond to periods with high freshwater input, including direct precipitation, resulting in strong salinity stratification that isolates bottom waters, allowing biological oxygen demand to draw down DO. Evidence indicates that lateral advection can contribute to reoxygenation events, and the relationship between near bottom DO and bottom salinities in the mid bay and back bay is consistent with deep-water renewal as the mechanism for bottom water ventilation. These hypoxia and temperature inversion events impact the biological communities of Bahía Almirante, and the physical dynamics that regulate these coincident and persistent stressors for marine organisms are likely present in other shallow, tropical estuaries.

Ocean deoxygenation is a prevalent phenomenon in many regions of the ocean (Diaz and Rosenberg 2008). Dissolved oxygen (DO) affects ecosystem function, biodiversity, and biogeochemistry in the ocean (Breitburg et al. 2018), and the number, intensity, and duration of hypoxic episodes is expected to increase due to the combined effects of ocean warming and eutrophication (Levin and Breitburg 2015). Hypoxia is commonly defined as DO $< 2 \text{ mg L}^{-1}$, but adverse effects for many species occur above this threshold (Vaquer-Sunyer and Duarte 2008).

Hypoxia is particularly common in estuarine and coastal waters (Gilbert et al. 2010) where both biogeochemical

Additional Supporting Information may be found in the online version of this article.

Author Contribution Statement: The observational study was designed by R.C. R.C., V.R., X.B., and A.E.A. managed the data. The analysis plan was designed by A.E.A. and G.P. with input from K.A.D., S.N.G., and R.C. Detailed analysis was carried out by A.E.A., A.G., and G.P. A.E.A. wrote the manuscript with contributions from A.H.A., R.C., K.A.D., S.N.G., and G.P. V.R. and A.G. commented on the manuscript.

processes including primary production and oxygen consumption (e.g., respiration and sediment uptake) and physical mechanisms (e.g., stratification, mixing, and advective transport) impact hypoxia development and breakdown. Eutrophication contributes to deoxygenation of coastal waters through organic material decomposition and associated microbial respiration and can lead to hypoxia (Breitburg et al. 2018). In estuaries and coastal waters, eutrophication is often linked to rivers laden with anthropogenic nutrients (Howarth 2008), but there are also natural mechanisms that deliver nutrientrich and/or oxygen-poor waters to continental shelves (Diaz and Rosenberg 2008), including upwelling (Chan et al. 2008) and watersheds with naturally high nutrient and organic matter (Wetz et al. 2006). Furthermore, conducive physical conditions can lead to hypoxia with or without excess nutrient inputs, such as water column stratification, water retention, or a combination thereof. Estuaries are often highly stratified such that a pycnocline isolates incoming, oceanic water from the outgoing, surface layer (Fennel and Testa 2019). When water column stratification inhibits bottom water ventilation

^{*}Correspondence: aeadelso@ucsd.edu

and there is no other mechanism for oxygen replenishment, hypoxia can develop, without nutrient additions.

Common mixing mechanisms that can contribute to coastal and estuarine bottom water ventilation, thus providing brief DO replenishment or full reoxygenation, include cooling convection (Boesch and Rabalais 1991), wind-driven mixing (Stanley and Nixon 1992), and tide-driven mixing (Kemp et al. 2009). Advection due to baroclinic longitudinal estuarine exchange and lateral circulation can also enhance vertical mixing and break down stratification (Smith 1976; MacDonald and Geyer 2004), thus impacting DO. Additional advective processes including variations in river inflows (Scully 2013) and deep-water renewal, commonly observed in fjords (Gade and Edwards 1980), also contribute to DO dynamics.

Hypoxia has been primarily documented in temperate coastal waters and estuaries (Diaz and Rosenberg 2008; Breitburg et al. 2018). Tropical estuaries are poorly studied relative to their temperate counterparts, and consequently there is inadequate data to elucidate the dynamics and function of tropical estuarine systems (Vieillard et al. 2020). Although low DO in deep tropical waters has been given some attention (Avendaño-Alvarez et al. 2017; Bates 2017; Kealoha et al. 2020; Scranton et al. 2014), few studies have focused on hypoxia in shallow tropical embayments. Ocean warming and acidification are frequently cited as threats to coral reefs, but there are still fundamental knowledge gaps in the role that low-DO levels and multiple stressors play in ecosystem health (Hughes et al. 2020), and a review of global literature by Altieri et al. (2017) suggests that dead zones in the tropics are likely severely under-reported, perhaps by an order of magnitude.

Although similarities to temperate regions exist, fundamental differences in tropical climate, oceans, and ecology suggests that alternate mechanisms may affect hypoxic events. For example, there are salient differences in nutrient cycling (Vieillard et al. 2020). In addition, solar radiation and rainfall are high and exhibit weak seasonal patterns relative to temperate regions (Nittrouer et al. 1995). These factors can contribute to stratification patterns, and can thus affect mixing and DO dynamics. In addition, warm temperatures increase microbial respiration associated with organic material decomposition (Pomeroy and Wiebe 2001). Thus, while the mechanisms that regulate tropical DO dynamics are similar to temperate systems, there are tropics-specific contributors that can modify these factors.

Tropical coral reef environments typically have high water clarity, and consequently, incident shortwave radiation can penetrate deep into the water column. Wells et al. (2012) observe bottom waters that warm quickly, leading to temperature inversions that are maintained by salinity stratification. Thermal stress at depth has been observed in tropical systems (Neal et al. 2014) and can co-occur with, and exacerbate the effects of, hypoxia (Vaquer-Sunyer and Duarte 2011). Tropical ecosystems are generally oligotrophic and may be more vulnerable to the detrimental effects of eutrophication (Corredor

et al. 1999), in part due to ecological feedbacks and thresholds in ecosystem state (Altieri et al. 2021). The paucity of comprehensive DO observations in the tropics demonstrates a critical need for understanding hypoxic events dynamics in order to predict and, if possible, mitigate the effects on corals and other foundation species. This study aims to examine physical mechanisms that impact the evolution of hypoxia in a tropical estuary that differ from temperate systems, including precipitation patterns and a surface heat budget, and the role they play in the hypoxia evolution and breakdown.

In this paper, we examine over 10 consecutive years of hydrographic data documenting recurring seasonal hypoxic events in a semi-enclosed tropical embayment in the Bocas del Toro Archipelago on the Caribbean coast of Panama. This analysis highlights the physical processes that are important in regulating hypoxia and temperature inversions in Bahía Almirante (Fig. 1). We aim to (1) document the patterns of seasonal variation in physical parameters, including temperature, salinity, and DO and (2) use these patterns to shed light on the likely physical mechanisms impacting the development and breakdown of hypoxia.

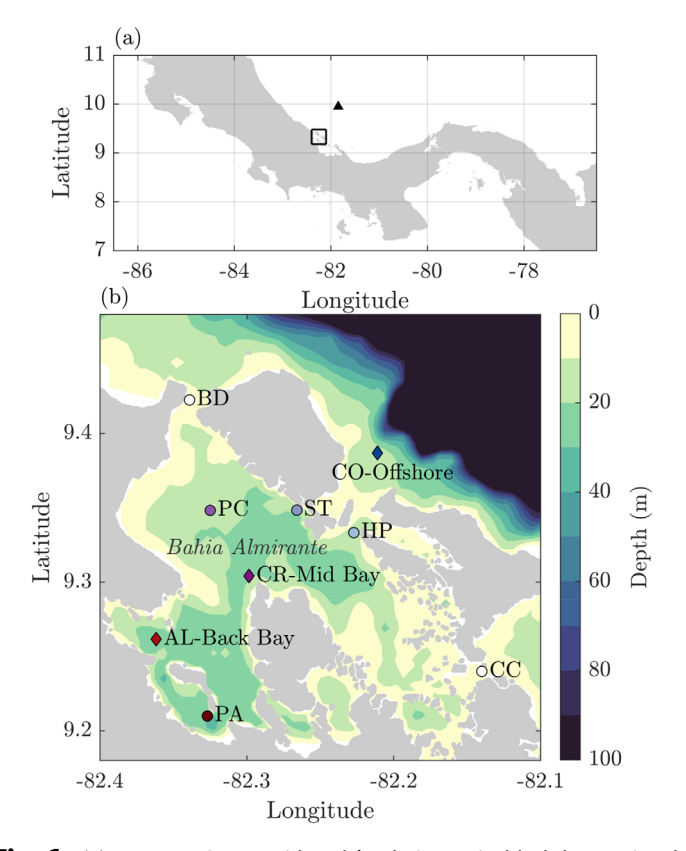


Fig. 1. (a) Panama Coast, with Bahía Almirante in black box. Triangle indicates location of ECMWF winds. (b) Weekly monitoring sites, colored by distance from offshore (blues) to the back bay (reds), used in subsequent figures. Diamonds indicate sites used to represent the bay regions in Fig. 3. ST is also the location of the local meteorological station. Bathymetry in color (GEBCO 2014). Sampling sites not used in this analysis are sh4.own in white.

Seasonal hypoxia in a tropical bay

Methods

Site description

Bahía Almirante's area is approximately 500 km², and the watershed is comprised of an equivalent area, although approximately half of it is coastal wetlands (Kaufmann and Thompson 2005). The bay's ecosystems include mangroves, seagrass beds, and patch reefs (Collin 2005). Previous work has noted pronounced haloclines in Bahía Almirante resulting from high rainfall (3 m yr⁻¹) and river runoff, with a top layer of low-salinity, typically cooler water transitioning sharply to a bottom layer of warmer water with near oceanic salinity (Kaufmann and Thompson 2005). A 2D (depth uniform) modeling study of Bahía Almirante linked horizontally spatially variable flow patterns and residence times to sea surface temperatures within regions of the bay (Li and Reidenbach 2014). Regional nutrient dynamics are poorly understood, but low nitrogen and phosphorus levels indicate that primary productivity in Bahía Almirante is nutrient limited (D'Croz et al. 2005), suggesting that eutrophication would meaningfully change the biological system. A recent study of river water quality in the Bahía Almirante watershed suggests that urban point source contributions are a more important nutrient source for the bay than riverine discharge (Clark et al. 2022).

Water properties in Bahía Almirante are affected by offshore ocean conditions through its multiple inlets. The bay has three major channels: Boca del Drago and Canal de Bastimentos connect Bahía Almirante to the open ocean and Cayo Coral opens into Laguna de Chiriqui (Fig. 1). Offshore water temperature and salinity are affected by the migration of the Intertropical Convergence Zone (ITCZ), the propagation of atmospheric tropical waves through the Atlantic basin, and variations in weather patterns (Kaufmann and Thompson 2005). The key circulation feature offshore is a southeastward surface flow associated with the cyclonic Panama-Colombia gyre. There is debate on the persistence of this feature (Andrade and Barton 2000), although Centurioni and Niiler (2003) observed strong cyclonic flow based on 5 yr of drifter observations. The Caribbean Sea has a well-mixed surface layer extending to 50 m, overlying a region (50-250 m) with strong stratification (Gallegos 1996).

Bahía Almirante's ecosystems face common coastal threats, including thermal, photic, and physical stresses. Persistent temperature inversions have led to increased thermal stress at depth (Neal et al. 2014). Bahía Almirante has experienced low-oxygen events combined with warming, leading to widespread bleaching and mortality of corals and other marine invertebrates (Neal et al. 2014; Altieri et al. 2017). In addition to the lethal effects of hypoxia, a recent experiment shows that some organisms, including sea urchins, exhibit measurable sublethal changes in performance when subjected to oxygen levels that reflect hypoxic conditions in Bahía Almirante (Lucey et al. 2020).

Data description

This analysis uses data from the Smithsonian Tropical Research Institute's (STRI) Physical Monitoring Program at the

Bocas del Toro Research Station in Panama (Paton 2020). STRI has collected air temperature, wind speed and direction, solar radiation, relative humidity, sea surface height, and water temperature data at a meteorological station (9.35°N, 82.26°W; Fig. 1), from 17 June 2002 to present. Values from June 2002 to April 2005 were recorded hourly. Beginning in June 2005, variables were measured every 10 s with average values recorded every 15 min. The European Centre for Medium Range Weather Forecasts (ECMWF) reanalysis product winds and total precipitation approximately 90 km offshore in Mosquito Gulf (9.95°N, 81.85°W; Fig. 1) provide regional meteorological context.

STRI has conducted a spatial sampling program from October 2010 to present. Nominally weekly vertical water column profiles of salinity, temperature, and DO were collected at sites around Bahía Almirante (Fig. 1). Seven sites were regularly visited (Almirante, Cristobal, Hospital Point, Pastores, Punta Caracol, and STRI within the bay; and Colon just offshore), and in 2019, a site near the channel at Boca del Drago was added. Measurements were taken in the same order at approximately the same time of day for each site, generally between 08:00 and 13:00 local time. Because the survey sites were sampled from offshore to onshore, there is some potential for diurnal aliasing. As a point of reference, data collected by a near-surface, moored YSI multiparameter sonde at STRI, located in shallow water near dense communities of seagrass, indicates that, on average, over the typical sampling period, water temperature increases by 0.5°C due to solar heating, and DO increases by 0.7 mg L^{-1} due to photosynthesis. This provides an upper bound for near-surface bias, with smaller changes expected at depth.

Before May 2015, samples were collected at four discrete depths (0.5, 5, 10, and 20 m) via bottle samples. Since May 2015, vertical profiles were measured using an YSI multiparameter sonde, including an optical DO sensor. Salinity accuracy is 1.0% of reading or 0.1 ppt (whichever is greater), temperature accuracy is 0.01°C, and DO accuracy is $\pm~0.1~mg~L^{-1}$ or 1% of reading, (whichever is greater). Because profiles were not uniformly steady, profile data were averaged into 2 m bins and weighted by the vertical distance between measurements. When possible, only the downcast was considered, unless there was only an upcast (1% of casts). Density was calculated from measured salinity, temperature, and depth using Gibbs Seawater toolbox of TEOS-10 (McDougall and Barker 2011). Values with a negative stratification were excluded (1.6% of casts). Annual averages for all parameters were computed using semimonthly means (24 equally spaced time bins per year).

Surface heat flux calculation

To assess bulk contributions due to advective heat fluxes, the net surface heat flux (Q_{SHF}) was calculated by estimating the shortwave (Q_{SW}) , longwave (Q_{LW}) , sensible (Q_S) , and latent (Q_L) heat fluxes, where

19395590, 2022

Adelson et al.

$$Q_{SHF} = Q_{SW} + Q_{LW} + Q_S + Q_L. \tag{1}$$

Shortwave heat flux was estimated using measured solar radiation, Q_{meas} , modulated by the sea surface albedo, α .

$$Q_{SW} = (1 - \alpha)Q_{\text{meas}}.$$
 (2)

Albedo was estimated via atmospheric transmittance and sun altitude, following Payne (1972). Longwave heat flux was calculated following Talley (2011) and Johnson et al. (2018) using observed sea surface temperature, air temperature, and water vapor. The method incorporates fractional cloud cover, estimated from satellite observations of cloud data from NASA's Clouds and the Earth's Radiant Energy System (CERES) project (NASA/LARC/SD/ASDC 2015). Latent and sensible heat fluxes were computed using sea surface temperature, surface air temperature, wind speed, and relative humidity using the package developed by Pawlowicz et al. (2001) (algorithm from Fairall et al. 1996). Shortwave, latent, and sensible heat flux time series were calculated at 15 min intervals, while the longwave heat flux was calculated hourly.

Results

Meteorological conditions

Regional winds in Mosquito Gulf, approximately 90 km offshore, reflect seasonal nominally northeasterly trade winds that weaken during the northern phase of the ITCZ (Andrade and Barton 2000), with seasonal average magnitudes up to $2.75~{\rm m~s^{-1}}$ (Fig. 2f). The local seasonal average winds are similar in magnitude (Fig. 2a) and are steered by the Cordillera de Talamanca, mountains approximately 60 km to the west which reach altitudes greater than 3400 m. The regional and local winds are maximum in January through March, and minimum in August through October, with a second, smaller wind peak in July.

There is significant freshwater influx to the bay through year-round precipitation, with moderate seasonality exhibiting precipitation increases in June through August and November through January (Fig. 2b). The phasing is similar to the wind peaks (Fig. 2a). Because Bahía Almirante's watershed is similar in area to the bay, roughly half of the freshwater input is expected to occur through direct precipitation, with the relative amount determined by the size of the bay vs. the watershed. Offshore precipitation (Fig. 2g) has a dry season from January to April and a rainy season from June to December.

Hydrography for Bahía Almirante

Similar to most estuarine systems, salinity is the most important parameter setting density stratification in the bay. The thermal contribution to density is on average approximately 11% of the salinity contribution. All sites exhibit vertical salinity stratification, including the offshore site (Figs. 2c, h, 3a,b,c). The lowest surface salinities are typically observed in the back bay, increasing slightly toward the mid bay, with higher surface salinities offshore (Fig. 3a–c). Back bay salinities

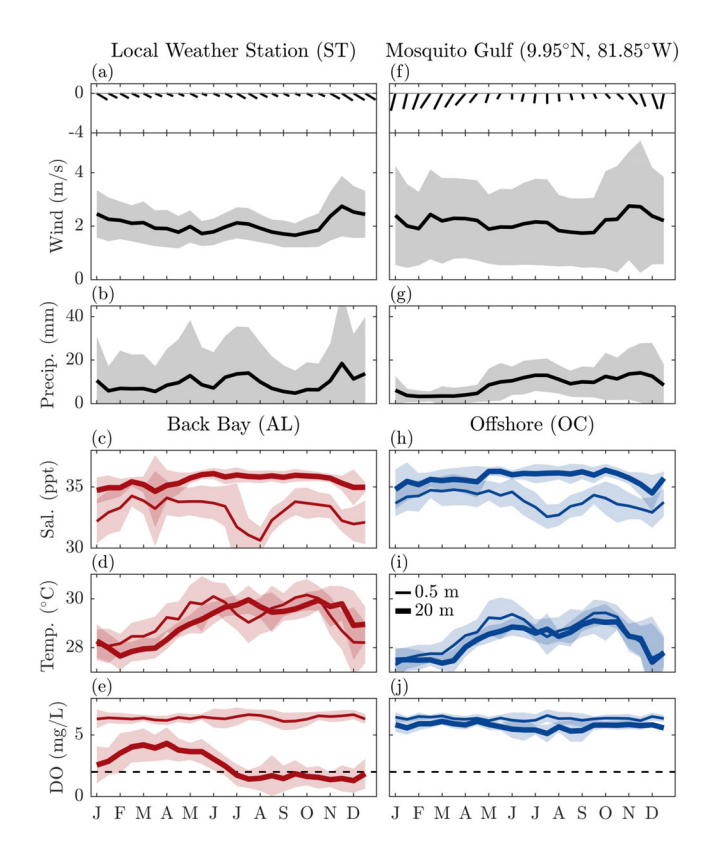


Fig. 2. Climatologies for meteorological and hydrographical variables averaged in half month intervals: **(a)** local winds measured at STRI, and local root-mean-squared wind speed magnitude (black line); **(b)** precipitation at STRI (2002–2019); **(c–e)** STRI sampling data for Almirante (a back bay site, Fig. 1) with **(c)** salinity; **(d)** temperature; **(e)** DO; **(f)** offshore (9.95°N, 81.85°W) regional wind speed and direction and **(g)** total precipitation from ECMWF (ERA5, 2010–2020); **(h–j)** STRI sampling data for Colon (offshore site; Fig. 1) for **(h)** salinity; **(i)** temperature; **(j)** DO. In **(c–e)** and **(h–j)**, 0.5 and 20 m are shown by light and heavy lines, respectively. Patches in all panels indicate ± 1 standard deviation; 2 mg L⁻¹ DO line (dashed) is shown for reference in **(e,j)**.

at depth are similar to, and occasionally exceed, the salinity at the offshore location. At 20 m, on average, the salinity difference between the bay sites and offshore is within 0.3–0.4 ppt. There are seasonal cycles in both surface and bottom salinities within the bay and thus in the water column stratification (Fig. 2c,i). Surface salinities reach minimums in July/August and December/January, corresponding to periods with high precipitation (Fig. 2b). The seasonal signal in salinity at 20 m is much weaker, with slight reductions from October to April, following offshore salinity (Fig. 2c,i).

Water temperatures in Bahía Almirante have an average of 28.9°C with slightly cooler temperatures offshore (Figs. 2d,i, 3d–f). The seasonal cycle dominates variability with the range and phasing consistent with values reported by Kaufmann and Thompson (2005). Two seasonal peaks in the average surface temperatures (back bay; Fig. 2d,g) coincide with each solar radiation maximum, while the 20 m temperature peaks lag the surface by approximately 1 month within the bay. The

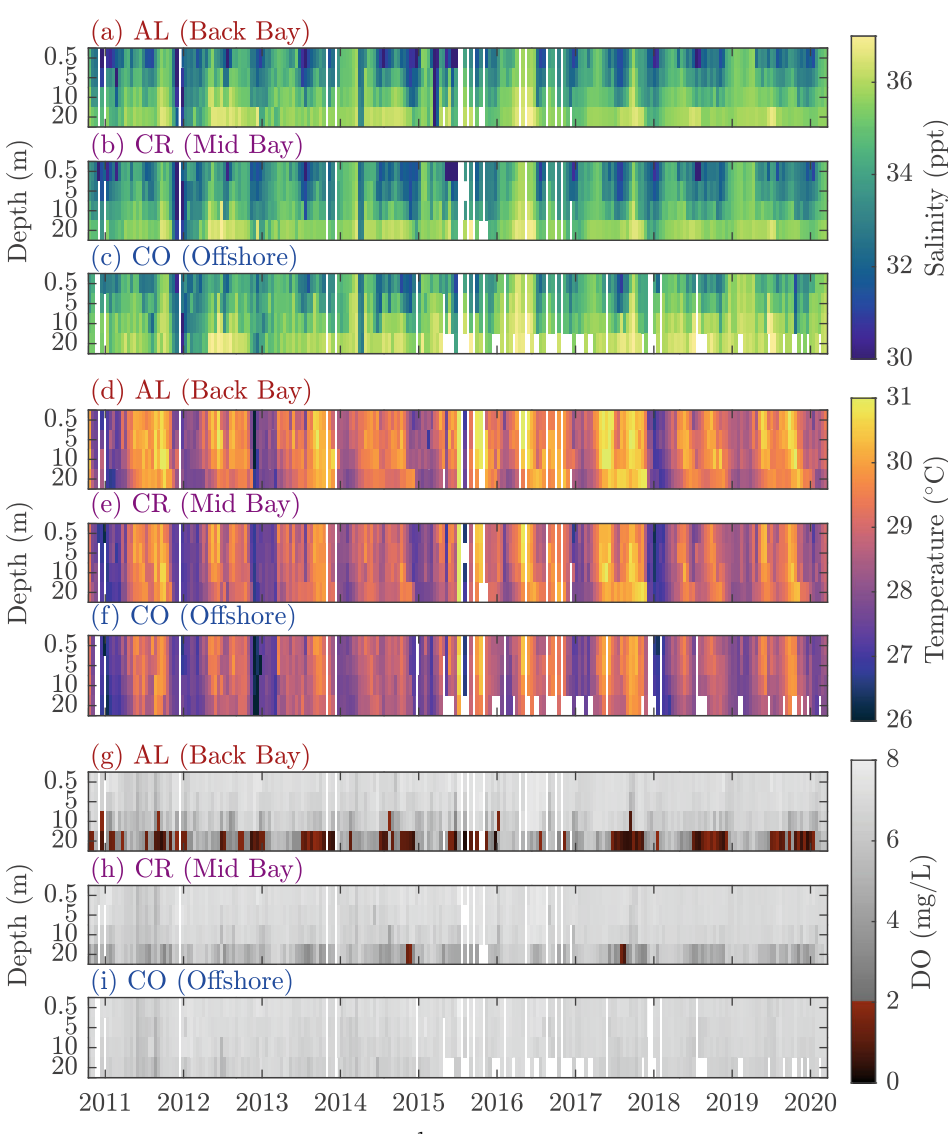


Fig. 3. Salinity (ppt) (\mathbf{a} – \mathbf{c}), temperature (°C) (\mathbf{d} – \mathbf{f}), and DO (mg L⁻¹) (\mathbf{g} – \mathbf{i}) from water sample measurements (bi-weekly bins) at four discrete depths (0.5, 5, 10, and 20 m) at three of the survey sites, indicated with diamonds on Fig. 1. Almirante (\mathbf{a} , \mathbf{d} , \mathbf{g}) represents the back bay, Cristobal (\mathbf{b} , \mathbf{e} , \mathbf{h}) represents the mid bay, and Colon (\mathbf{c} , \mathbf{f} , \mathbf{i}) represents offshore conditions.

temperature maxima phasing is coincident with the formation of seasonal temperature inversions, with temperature at depth exceeding surface temperatures in July/August and November/ December in the back bay (Figs. 2d, 3d–f). Seasonal temperature inversions are generally strongest in the back bay, decreasing in strength in the mid bay, and further weakened offshore (Fig. 2d,i). Although increasing inversion strength weakens vertical stratification, the strongest temperature inversions are typically accompanied by strong bulk salinity gradients that maintain water column stability.

DO levels throughout Bahía Almirante vary and are typically normoxic. The critical exceptions are severe DO reductions that occur seasonally at depth (Figs. 2e, 3g,h). On average, DO levels at depth begin to decline in May and reach hypoxic levels ($< 2 \text{ mg L}^{-1}$) in July (Fig. 2e). Hypoxia can

persist until bottom water ventilation occurs in December/ January (Fig. 2e). The time series at each of the three sites along the onshore-offshore line (Fig. 3g–i) depict a pronounced spatial pattern of hypoxia in Bahía Almirante. Hypoxia occurs with the greatest regularity, intensity, and persistence in the back bay (Fig. 3g), where DO reductions also occur at shallower depths. Corresponding seasonal DO declines are observed in the mid bay (Fig. 3h), although these events rarely reach the 2 mg L $^{-1}$ threshold and exhibit greater intermittency than the back bay. Offshore, hypoxia is never observed, and while weak DO declines occur at depth in June–September, values typically remain greater than 5 mg L $^{-1}$. There is no significant, long-term DO trend. Although there is a strong seasonal pattern (Fig. 2e), all sites demonstrate considerable interannual variability in the intensity, spatial

extent, persistence, and depth of hypoxic waters in Bahía Almirante. For further exploration of the year-to-year variations in hypoxia (Supporting Information Figs. S1, S2) and temperature inversions (Supporting Information Table S1), see the Supporting Information.

The spatial pattern evident in the data may be somewhat muted by the diurnal aliasing of the measurements, noted earlier. The offshore site is measured at an earlier point in the diel cycle than the back bay sites such that DO and water temperature will be relatively lower. This tends to counteract the spatial trend observed in the data. Tidal aliasing may also impact the measurements, but its effect is expected to be small because of the small tidal range and phase shift between the diurnal cycle and the tides.

Seasonal and spatial patterns in hypoxia and temperature inversions

We examine the measurement period with higher vertical resolution (2015–2020) to provide a more comprehensive look at the variability and vertical structure of hypoxia and temperature inversions (Fig. 4). The timing of the hypoxic season changes from year

to year, with hypoxia onset typically occurring between May and July and bottom water ventilation between late December and February. Intermittent recoveries are common, particularly in the mid bay where few hypoxic episodes last more than a few consecutive weekly measurements (Supporting Information Fig. S1).

At all interior sites, average subsurface DO is reduced during hypoxic periods (Fig. 4d); however, DO reductions are most extreme in the back bay (Almirante and Pastores; Fig. 3g-i, 4a), where individual measurements are lower than 0.1 mg $\rm L^{-1}$ (the instrument accuracy limit) and individual hypoxic measurements reach depths as shallow as 7 m. The average DO profiles for the hypoxic period in the mid bay (Cristobal, Hospital Point, Punta Caracol, STRI) exhibit minimum average levels as low as 3 mg $\rm L^{-1}$ (Fig. 4d), a threshold known to have sublethal effects (Vaquer-Sunyer and Duarte 2008). The offshore site remains normoxic and shows little variation between the hypoxic and normoxic periods. During the normoxic period, the mid bay sites exhibit DO profiles similar to offshore, while the back bay has reduced DO (Fig. 4d,e).

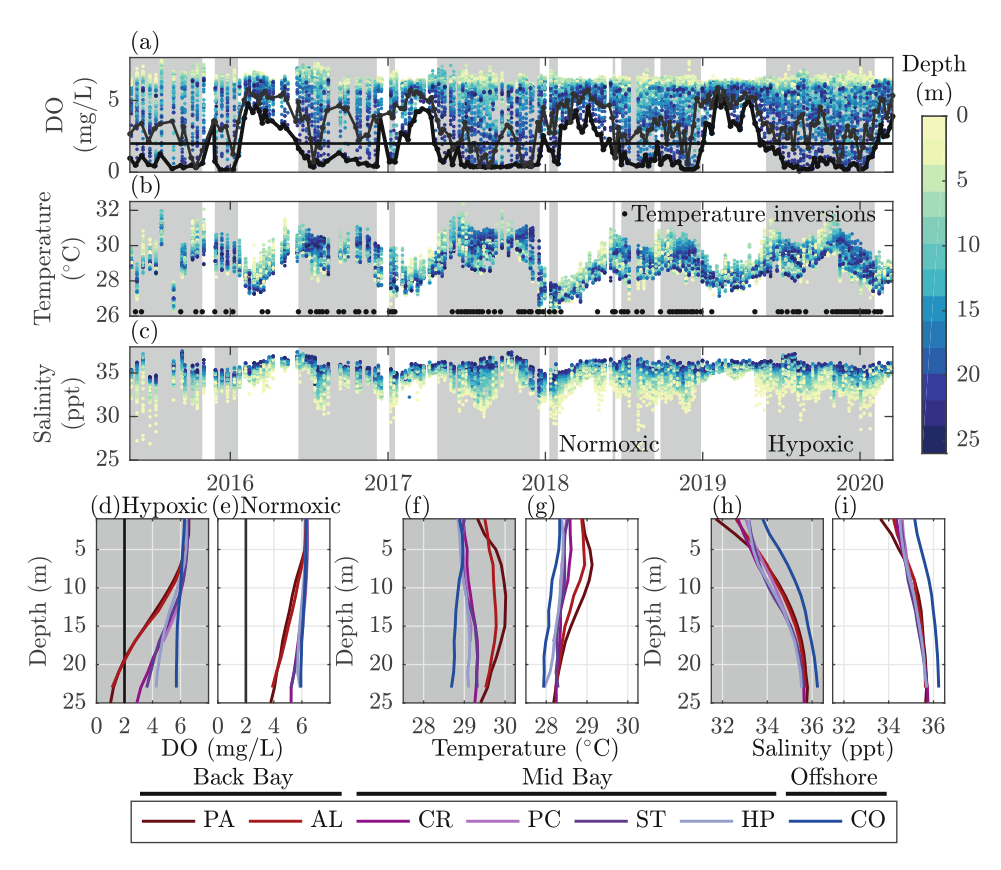


Fig. 4. Profile time series from May 2015 to March 2020, at interior Bahía Almirante sites (all sites excluding offshore), with depth in color. Gray background indicates periods when at least one site is hypoxic ($DO < 2 \text{ mg L}^{-1}$), defined as the hypoxic period, whereas a white background indicates normoxic measurements ($DO > 2 \text{ mg L}^{-1}$) at all sites, defined as the normoxic period. (**a**) $DO \text{ (mg L}^{-1})$, heavy black line: minimum DO; thin gray line: minimum $DO \text{ excluding two back bay sites (Pastores and Almirante). ($ **b** $) Temperature (<math>^{\circ}C$), black dots denote profiles with a temperature inversion greater than $1^{\circ}C$ anywhere in the water column; (**c**) salinity (ppt); (**d-i**) show ensemble average vertical profiles at each site during hypoxic (**d,f,h**) and normoxic (**e,g,i**) conditions for DO (d,e), temperature (**f,g**), and salinity (**h,i**). Sites are labeled in color as in Fig. 1 and as identified in the legend. $DO \text{ mg L}^{-1}$ DO line is shown for reference in (**a,d,e**).

Water temperatures tend to be warmer during the hypoxic periods relative to the normoxic periods (Fig. 4b,f,g). Temperature inversions greater than 1°C commonly occur during the hypoxic period (Fig. 4b, black dots) but are infrequent during the normoxic periods. Temperature inversions tend to occur in the mid water column, where hypoxic-period ensemble average temperatures can exceed 30°C (Fig. 4e). The warmest temperatures occur in the back bay, with the mid-water column 1.1°C warmer than offshore and 0.8–0.9°C warmer than the other monitoring sites. Although the thermal spatial gradient is diminished during the normoxic period, the back bay sites continue to exhibit temperature profiles that are warmer than the rest of the bay and that have near surface (< 8 m) temperature inversions.

The lowest surface salinities occur during the hypoxic period (Fig. 4c,h,i), indicating stronger stratification. In addition, there is a spatial gradient in surface salinity, especially during the hypoxic period, leading to a horizontal gradient in vertical stratification, amplified during the hypoxic period, as average salinities at 20 m within the bay are consistent between the hypoxic and normoxic periods.

Seasonal hypoxia (Fig. 5a) and temperature inversions (Fig. 5b) follow similar spatial patterns; they are most intense and frequent in the back bay, where stratification is strongest, and decrease offshore. The offshore site and the site closest to a channel (Hospital Point) never experience hypoxia, while all sites experience temperature inversions during both the hypoxic and normoxic periods. The normoxic period typically has stable temperature stratification, with inversions in less than

5% of measurements at each site (Fig. 5b, right bubble). During the hypoxic period, all sites experience higher incidences of temperature inversions, and all, except the offshore site, exhibit a bulk temperature inversion in the ensemble average (Fig. 5b, left bubble).

Dynamical drivers and co-occurrence of DO and temperature inversions

In order to develop a dynamical framework for hypoxia in Bahía Almirante, we consider physical environmental factors that influence hypoxia development and breakdown. This section examines evidence that high vertical stratification corresponds to low DO, temperature inversions, and high temperatures at depth. Lagged correlations are examined to explore the temporal relationships between environmental factors and water properties. The sampling interval prohibits consideration of lags shorter than 1 week; however, the time series length enables consideration of the relationships between parameters on weekly and longer time periods and provides a bulk sense of the dynamics in Bahía Almirante. Lags of up to 5 weeks were considered. Unless otherwise noted, the maximum correlation occurs with no lag. Confidence intervals found via bootstrapping (n = 1000) provide error bounds on the correlations and linear fits. Although binned mean values are shown for illustrative purposes, all correlations reported correspond to raw data.

The dominant role of salinity on density variations in the bay suggests that precipitation will be important in determining vertical stratification. There is a statistically significant,

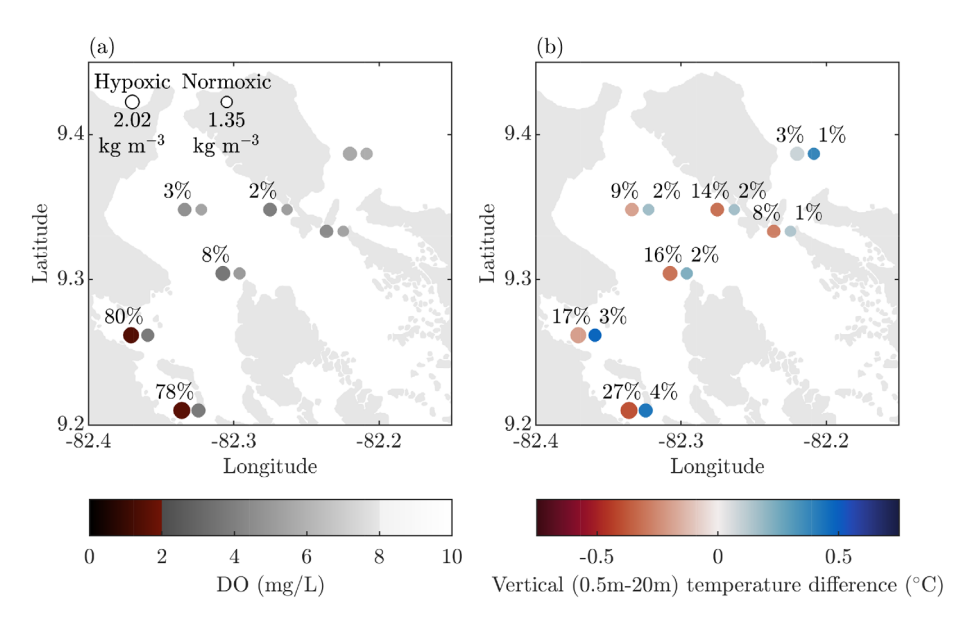


Fig. 5. Spatial patterns of ensemble averages of: (a) DO at 20 m (indicated by color) during the hypoxic period (left bubble) and normoxic period (right bubble), as defined in Fig. 4. Percentages indicate fraction of measurements that are hypoxic. If there are no incidents of hypoxia (i.e., 0%) the percentage is not included. (b) Vertical (0.5–20 m) temperature difference (indicated by color) during the hypoxic period (left bubble) and normoxic period (right bubble). Red indicates temperature inversions. Percentages indicate percent of measurements that have vertical temperature differences greater than 1°C. Bubble size in both panels is scaled by the top-bottom density difference, with larger bubbles indicating greater stratification. Legend in (a) provides references of spatial-average, ensemble-averaged top-bottom density difference for the hypoxic and normoxic periods.

weakly positive correlation (r = 0.24; p < 0.05) between weekly precipitation and vertical density difference lagged by 1 week (Supporting Information Fig. S3). The 1 week lag indicates that precipitation history is relevant and may also reflect a temporal delay in riverine freshwater inputs, although this delay may be between 1 d and 1 week. There is no statistical relationship between wind and vertical stratification.

The statistically significant negative correlation (r = -0.51; p < 0.05) between vertical stratification and DO indicates that low DO is linked to greater stratification (Fig. 6a). Conversely, when the vertical density difference is weak, bottom waters are more likely to be oxygenated.

There is also a statistically significant negative correlation (r = -0.38; p < 0.05) between vertical stratification and the magnitude of the most negative vertical temperature

gradient normalized by its depth interval, $\min(\delta_z T)/\delta z$ (Fig. 6b). This indicates that temperature inversion strength also increases with increased stratification. Temperature inversions co-occur with lower DO concentrations, while no clear relationship is evident between DO and positive min $(\delta_z T)/\delta z$ (Fig. 6c). This statistically significant relationship is not interpreted as causal because it is most likely a result of temperature inversions and hypoxia resulting from related dynamical conditions, in this case increased salinity stratification (Fig. 6a,b).

Using a technique developed by Goreau and Hayes (1994) to identify potential areas of coral bleaching based on satellite data, "hot spots" can be identified by regions with sea surface temperatures at least 1°C greater than the highest (i.e., warmest) monthly mean. The highest monthly baywide-mean

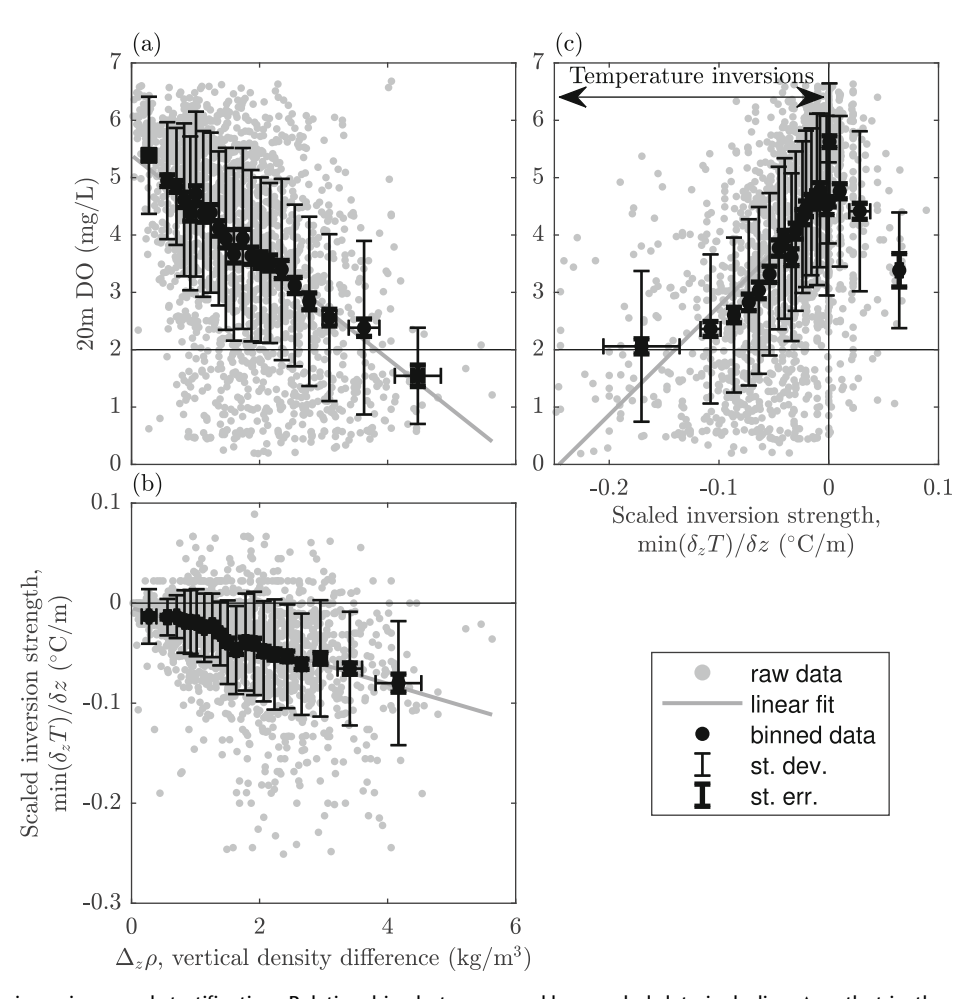


Fig. 6. DO, temperature inversions, and stratification: Relationships between weekly sampled data including Δ_{zP} , that is, the vertical (20–0.5 m) density difference (kg m⁻³), DO at 20 m (mg L⁻¹), and min($\delta_z T$)/ δz , that is, the most negative vertical temperature difference in the water column normalized by the difference in depths (°C m⁻¹), at the six interior sites. Outliers, absolute deviations greater than three scaled medians, are excluded. Gray points: raw data; black points: mean in 100 point bins; error bars: 1 standard deviation; heavy error bars: standard error. (**a**) 20 m DO vs. $\Delta_z P$: 35 outliers; 1.7%. For the raw data: r = -0.51; 95% confidence intervals = [-0.54 to 0.47], p < 0.05. Fit slope = -0.88; confidence intervals = [-0.95 to 0.82]. (**b**) min($\delta_z T$)/ δz vs. $\Delta_z P$: 122 outliers, 6%. For raw data with inversions (i.e., min($\delta_z T$)/ $\delta z < 0$; n = 1746), r = -0.38; 95% confidence intervals = [-0.41 to 0.33], p < 0.05. (**c**) DO vs. min($\delta_z T$)/ δz : 93 outliers; 4.4%. For raw data with inversions: r = 0.51; 95% confidence intervals = [0.48 0.54], p < 0.05. Fit slope = 19.0; confidence intervals = [17.3–20.6].

temperature in Bahía Almirante is 29.7 °C at both 0.5 and 20 m depth (Fig. 7, red line). As conditions approach the lower right quadrant of Fig. 7, organisms are more likely to experience metabolic stress. Eighteen percent of data exceed the highest monthly mean temperature, and 16% are below the 2 mg L⁻¹ hypoxia threshold, with 7% of the data occurring when both temperatures exceeds the highest monthly mean and DO falls below the hypoxic threshold (i.e., lower right corner of Fig. 7 defined by the red and black lines). At least one of these stressors is present for 27% of measurements. There are only eight data points (approximately 0.4% of all data) in the parameter space where thermal stress (exceeding the highest monthly mean temperature by $+ 1^{\circ}$ C; line not shown) co-occurs with hypoxic stress ($< 2 \text{ mg L}^{-1}$), as these benchmarks are defined. When considering only the back bay sites (Almirante; Pastores), 17% experience multiple stressors, and 1% of measurements exceed the highest monthly mean by $+ 1^{\circ}$ C. Although this is illustrative for potential implications for organisms, this analysis considers the bay as a whole and does not account for species-specific thresholds or spatial distribution, nor tolerance shifts due to the presence of multiple stressors.

Heat budget

High residence times can be conducive to deoxygenation, and lateral advection is a possible mechanism of bottom water ventilation. Analysis of the bay heat budget allows assessment of the role of advection, provides residence time estimates, and explores the spatial and seasonal variations to further understand the patterns previously described. Shortwave

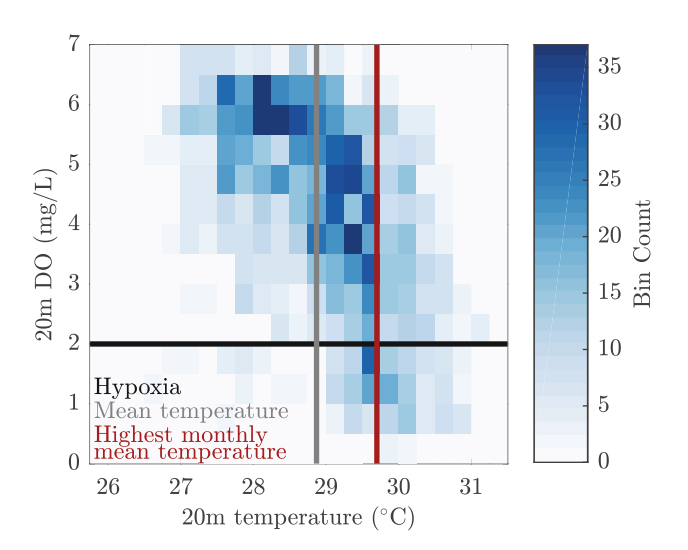


Fig. 7. Histogram of DO vs. temperature: 2D histogram of weekly sampled DO at 20 m (mg L^{-1}) vs. weekly sampled temperature at 20 m (°C) at the six interior sites. Reference lines include: 2 mg L^{-1} DO (black), baywide average temperature (gray), and highest monthly mean temperature (red). Temperature bin widths: 0.5 °C, DO bin widths: 0.5 mg L^{-1} .

radiation (Q_{SW}) dominates the net surface heat flux (Q_{SHF}) , with peaks that occur during the solar maxima for the tropics (Fig. 8a). Notably, there is an input of heat throughout the year.

A simplified integral heat budget for a control volume can be written as:

$$\langle \overline{\rho} \rangle C_{\rm p} h A \frac{\Delta \langle \overline{T} \rangle}{\Delta t} = \overline{H}_{\rm S} + \overline{H}_{\rm A}.$$
 (3)

Here C_p is the specific heat capacity (in units J K⁻¹ kg), h is the average water depth, and A is the surface area. <> represents a volume average for the region of interest, and the overbar indicates temporal averaging over a time scale Δt , such that $\langle \overline{\rho} \rangle$ and $\langle \overline{T} \rangle$ are the volume- and time-averaged density and temperature, respectively, $\overline{H}_{\rm S} = \overline{Q}_{\rm SHF} A$ is the net surface heat flux integrated across the surface, and $\overline{H}_{\rm A}$ represents the net heat contribution due to all advective sources. The latter can include lateral fluxes across boundaries, input from rivers and heat fluxes due to precipitation.

The integrated heat budget in (3) then yields the temporal change in the bulk temperature which can be decomposed into surface heat flux and advective components:

$$\Delta \langle \overline{T} \rangle = \Delta \langle \overline{T} \rangle_{S} + \Delta \langle \overline{T} \rangle_{A}. \tag{4}$$

The weekly temperature change for a particular region, $\Delta\langle\overline{T}\rangle$, can be estimated using the weekly sampling observations, with $\Delta t=1$ week. The contribution due to the surface heat flux, $\Delta\langle\overline{T}\rangle_{\rm S}=\overline{Q}_{\rm SHF}\Delta t/(\langle\overline{\rho}\rangle C_{\rm p}h)$, can be estimated from the weekly averaged heat flux quantities (as described in "Methods" section). The change in temperature due to the advective flux, $\Delta\langle\overline{T}\rangle_{\rm A}=\overline{H}_{\rm A}\Delta t/(\langle\overline{\rho}\rangle C_{\rm p}hA)$, is then estimated as the residual.

Figure 8b shows the annual average variations in the baywide (average of interior bay sites) weekly temperature change along with variations in $\Delta\langle \overline{T}\rangle_{\rm S}$ and the residual, $\Delta\langle \overline{T}\rangle_{\rm A}$, using Eq. (4). $\Delta\langle \overline{T}\rangle_{\rm S}$ has two peaks in expected temperature increase and is positive throughout the annual cycle, reflecting the net surface heat influx. The observed temperature is consistent with a largely steady state thermal balance with periods of increasing and decreasing temperatures that are in phase with the surface flux. The difference, $\Delta\langle \overline{T}\rangle_{\rm A}$, reflects a net outward advective heat flux (Fig. 8b, orange line). Bahía Almirante thus acts as a net exporter of heat, consistent with the higher bay temperatures and as would be necessary to compensate for the net input at the surface, as is common at the tropics.

Precipitation and river flow contributions to the advective heat flux associated can be shown to be negligible, using observed rain estimates with reasonable temperature values. We assume that the advective heat flux is primarily through the three main channels (Fig. 1) and can be written in terms of a time-averaged effective exchange volume flux $\overline{\Gamma}$, as

$$\overline{H}_{A} = 2\langle \overline{\rho} \rangle C_{p} \Delta T_{X} \overline{\Gamma}, \qquad (5)$$

where $\Delta T_X = \overline{T}_{\rm CO} - \langle \overline{T} \rangle$ is the temperature difference between the interior bay and the offshore site, Colon. Using (5), we can calculate $\overline{\Gamma}$ as

$$\overline{\Gamma} = \frac{\Delta \langle \overline{T} \rangle_A}{2\Delta T_X} \frac{hA}{\Delta t}.$$
 (6)

where $\Delta \langle \overline{T} \rangle_A$ is estimated using (4). This estimate of $\overline{\Gamma}$ indirectly incorporates the turbulent and tidal fluxes.

The seasonal variation in ocean-bay temperature difference, ΔT_X , remains negative over the year (on average, about -0.5° C; not shown) and is fairly constant, consistent with heat export. The resulting effective volume exchange $\overline{\Gamma}$ (not shown) then follows the pattern for $\Delta \langle \overline{T} \rangle_A$ (Fig. 8b).

We can estimate a bulk residence time (t_r) for the bay using $\overline{\Gamma}$ as:

$$t_{\rm r} = \frac{hA}{\overline{\Gamma}} = \frac{2\Delta T_X \Delta t}{\Delta \langle \overline{T} \rangle_{\rm A}}.$$
 (7)

There is no discernible seasonal pattern in $t_{\rm r}$ (not shown), but median monthly values in bulk residence times for the bay vary between 10 and 40 d. Residence times for subregions

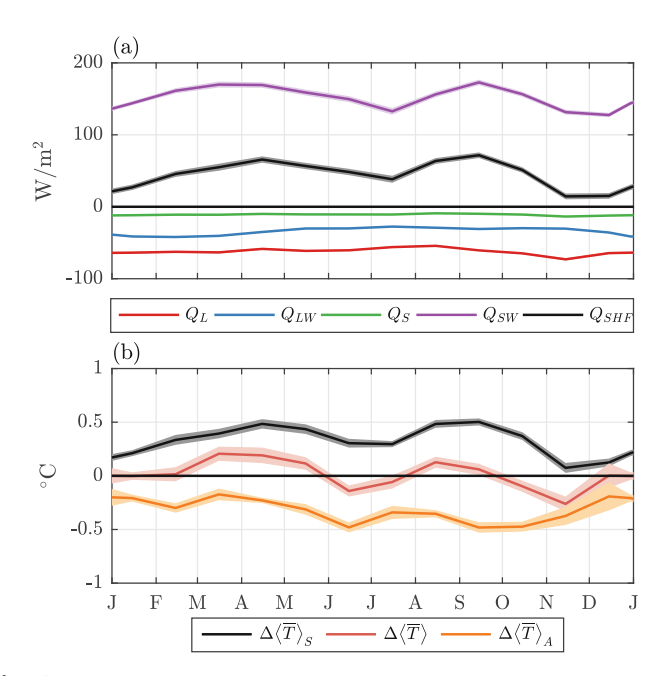


Fig. 8. Annual pattern for (**a**) surface heat flux (Q_{SHF} , black line) in Bahía Almirante, and its components: latent heat flux (Q_{L} , red line), long wave heat flux (Q_{LW} , blue line), sensible heat flux (Q_{S} , green line), shortwave heat flux (Q_{SW} , purple line). (**b**) the measured, normalized weekly change in water temperature ($\Delta\langle\overline{T}\rangle$, pink line), the weekly change in temperature due to the surface heat flux, assuming one-dimensional ($\Delta\langle\overline{T}\rangle_{S}$, black line), and the residual change in water temperature, assumed due to advection ($\Delta\langle\overline{T}\rangle_{A}$, orange line), where a positive value indicates heat transport into the bay and negative indicates heat export.

of the bay can similarly be calculated using Eq. 7 with appropriate volume averages, with the surface heat flux assumed to be the same in each region. Median values are given in Supporting Information Table S2 for the mid bay to offshore, back bay to offshore and the full bay to offshore. Estimates for the mid bay are lower, that is, shorter, than for the back bay as expected. The persistence of strong stratification and hypoxic events, especially at the back bay, reflects the spatial heterogeneity that is suggested by the residence time estimates, with shorter times near the entrances and much longer values toward the back bay, consistent with the results in Li and Reidenbach (2014).

Examination of a hypoxia breakdown event

The time series data in Figs. 3, 4 highlight considerable year-to-year and event-to-event variability, reflecting more complex dynamics associated with hypoxic event breakdown than is evident in the climatology. Here, we examine a specific breakdown event that illustrates potential mechanisms that can affect bottom water ventilation in Bahía Almirante.

At the start of the period considered, a deep hypoxic layer (time t_1 , 07 January 2016, Fig. 9b, dark red) is warmer than the rest of the water column and offshore (Fig. 9c, dark red) and has a higher salinity than the rest of the water column (Fig. 9d, dark red). This suggests an isolated bottom layer at t_1 , approximately 5–7 m thick. The bottom layer in the back bay is oxygenated by the next measurement, $(t_2, 19 \text{ January } 2016)$; however, the mid-water column is hypoxic (Fig. 9b; medium red), between 8 and 18 m. The temperatures and salinities in the mid-water column at t_2 are similar to those of the bottom layer at t_1 . The temperatures and salinities at depth are cooler and saltier at t_2 than t_1 . By 02 February 2016 (t_3), the water column is normoxic (Fig. 9b, light red), although there is remnant vertical structure in the DO profile. At t_3 , the water column is colder and saltier relative to t_2 in the back bay. Over the same time window, offshore water properties (Fig. 9c,d; medium blue, light blue) are also cooler and saltier, while DO remains normoxic. By t_3 , there is no meaningful temperature inversion and salinity stratification has weakened. Density profiles (not shown) indicate that the system is salinity stratified through this time period.

The time series of 3-h averaged wind speeds indicates that between t_1 and t_2 , wind speeds appear to be typical for this time of year, between 0.2 and 4.1 m s⁻¹, compared to the average range of 1.3 to 3.3 m s⁻¹ (Fig. 9a). Between t_2 and t_3 , there is a significant wind event, with wind speeds reaching 6.4 m s⁻¹, approaching the historical maximum for this time period.

In this example, the changes in deep-water properties in the back bay are consistent with advective processes, suggesting that offshore influences play a role in governing the system. The hypoxic layer at the back bay site appears to be replaced by a deep intrusion of water with higher salinity and lower temperature, consistent with properties from the

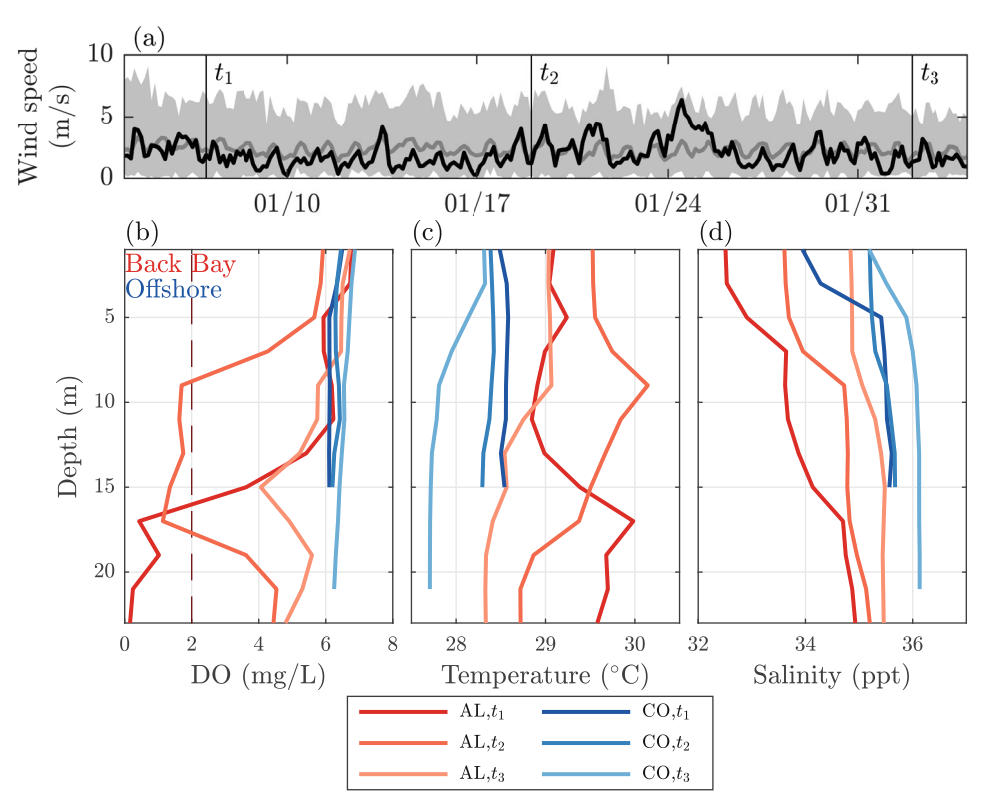


Fig. 9. January 2016 hypoxia breakdown. (a) Wind speed, 04 January 2016–04 February 2016 (black line), climatological mean (gray line), range over time series (gray shading), (b–d) profiles for (b) DO, (c) temperature, (d) salinity for Almirante (back bay, red) and Colon (offshore, blue). Time increases for lighter colors: 07 January 2016 (dark red and blue); 19 January (medium red and blue); and 02 February (light red and blue).

offshore site. The similarities between the water properties at depth during the first measurement (t_1) and in the mid-water column during the second measurement (t_2) suggest that the hypoxic layer was displaced upwards. It is notable that the deep-water ventilation is coincident with light winds between t_1 and t_2 . Changes near the surface are evident between t_2 and t_3 , though salinity at depth continues to increase indicating that wind-driven mixing from the wind event between t_2 and t_3 does not extend to the bottom layer.

Discussion

Analysis of the hydrography of Bahía Almirante reveals an estuarine structure with regular, seasonal hypoxia at depth, often coincident with temperature inversions, where both are more prominent toward the back of the bay. Hypoxia occurrence and temperature inversion events are correlated with seasonal changes in stratification. The following discussion examines the potential mechanisms for the onset and breakdown of hypoxic events.

Onset of hypoxic events

Freshwater inputs influence DO levels in Bahía Almirante via stratification. Conditions offshore remain normoxic

indicating that hypoxia develops within the bay. The precipitation increase that begins in April/May (Fig. 2b) is correlated with a surface freshening (Fig. 2c) leading to increased vertical salinity stratification (Supporting Information Fig. S3), even while salinity at depth remains high and sometimes exceeds offshore values. Because Bahía Almirante's watershed is relatively small, direct precipitation is a critical freshwater source (Clark et al. 2022). Freshwater inputs into canonical estuaries are dominated by rivers, leading to a horizontal density gradient that drives exchange flows. In contrast, Bahía Almirante's rivers are small and dispersed, largely along the mainland, and direct rainfall results in a broad freshwater capping layer that extends offshore, which may lead to reduced baroclinic advection and consequently increased flushing timescales relative to those for equivalent riverine inputs.

Stratification's critical role in the onset and evolution of hypoxia is consistent with observations in temperate estuarine and coastal systems (Stanley and Nixon 1992; Wiseman et al. 1997; Scully 2013). In Bahía Almirante, the drawdown of DO at 20 m typically begins around April and continues through August, coincident with the surface freshening (Fig. 2). This seasonal view further supports the idea that hypoxia develops after a period of elevated freshwater input which results in a strong, salinity-induced vertical

stratification with an isolated deep layer. Continued biological oxygen demand from the respiration of organic matter within this isolated layer leads to hypoxic conditions. It is possible that a seasonal cycle in respiration may contribute to the observed patterns in hypoxia; however, previous work indicates that there is not a seasonal signal in chlorophyll concentrations (Collin et al. 2009). The lack of seasonality in primary productivity in Bahía Almirante may be similar to other tropical, oligotrophic systems, as solar radiation weakly varies throughout the year.

This analysis has demonstrated that stratification in Bahía Almirante is adequately strong for the formation and maintenance of hypoxic events. Nutrient dynamics were not considered in this analysis, but they may play a role in seasonal hypoxia in the bay. Regional coastal land use changes include banana cultivation and development (Cramer 2013), and thus possible avenues for nutrient fluxes into Bahía Almirante include untreated sewage outfalls, river inputs, marine sources, groundwater, and atmospheric deposition. It can be inferred that nutrient loading would exacerbate the effects of the physical conditions that favor hypoxia (Rabalais et al. 2010), although the contribution of excess nutrients to hypoxia development in Bahía Almirante remains an open question. The precipitation patterns in Bahía Almirante that impact stratification, particularly the lack of a dry season, differ from other tropical regions; however, the seasonality in precipitation may also play a role in stratification, and thus DO dynamics, in other tropical estuaries.

Breakdown of hypoxic events

Despite interannual variability in the onset, duration, and termination of the hypoxic period, annual deoxygenation indicates that the driving forces of hypoxia also occur on a seasonal timescale. Seasonal averages (Fig. 2) and the time series data (Fig. 3) indicate that despite stratification weakening in September, hypoxia persists, occasionally for several months, suggesting that breakdown mechanisms, such as turbulent mixing or advection of oxygen-rich waters, are not present or strong enough in that period to ventilate deep waters. Seasonal hypoxia breakdown coincides with increased local and regional winds (Fig. 2), suggesting that wind-driven mixing may be an important factor, although analysis (not shown) indicated no statistical relationship between wind and DO time series. In addition, a strong wind event that followed one breakdown event resulted in surface mixing but did not affect bottom water (Fig. 9).

The high, near-bottom salinities observed in the back bay at the start of the event examined in Fig. 9 are consistent with the salinity climatology (Fig. 2c) and point toward a deepwater renewal hypothesis for hypoxia breakdown. This model is commonly associated with ventilation in fjords where dense, salty water is isolated in deep regions and can only be refreshed by sufficiently dense water in adequate supply at the sill (Gade and Edwards 1980). Deep-water renewal occurs

intermittently, typically when mixing of inflowing ocean water is weak and often varies on a spring-neap tidal cycle (Farmer and Freeland 1983; Silva and Vargas 2014). Deep-water renewal, governed by the monsoon and the spring-neap phase of the internal tide, has been observed in Ambon Bay, Indonesia, a shallow-silled, tropical fjord (Salamena et al. 2021). Analysis of event persistence in Bahía Almirante based on hypoxia thresholds yields timescales that are potentially consistent with fortnightly processes (Supporting Information Fig. S1), though the weekly sampling scheme precludes resolution of spring-neap processes.

Exchange fluxes and residence times inferred from the heat budget analysis indicate that advection in Bahía Almirante is significant and persistent. It is important to note that this analysis considers the bay (or its subregions) in a volume-averaged sense and thus variations in circulation within the bay remain unresolved. Significant portions of the mid and back bay are deeper than the entrance channels (Fig. 1). Ventilation of these deep regions requires advection of high-density water (relative to the back bay), thus a salty, deep layer in the back bay will remain isolated despite strong advection through the channels if the necessary inflow density condition is not met. Advection at the bay entrances alone is thus unlikely to be sufficient to ventilate the back bay.

The salinity climatology (Fig. 2c), which drives variations in density, provides an explanation for the seasonality in advection-driven hypoxia breakdown. Offshore salinity remains high throughout the year at depth, while surface salinity varies approximately coincident with the hypoxia cycle (and roughly following seasonal precipitation). If we postulate a persistent mechanism for vertical mixing of incoming offshore water, associated with energetic flow through the channel entrances, tidal or otherwise, then the density of the inflowing layer will be reduced in proportion to the vertical stratification. Following this

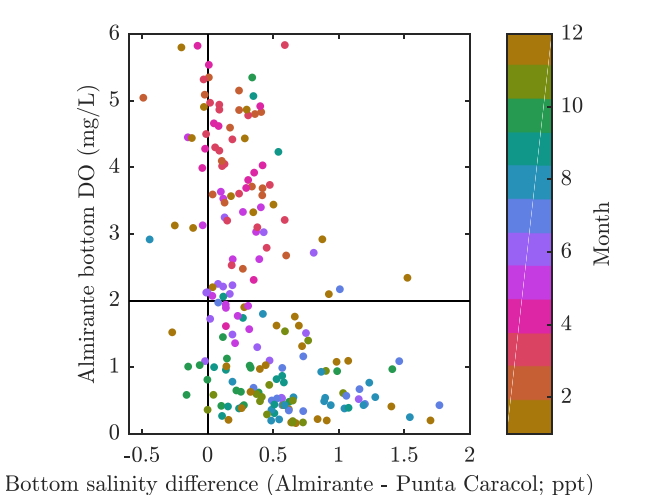


Fig. 10. Almirante bottom DO vs. bottom salinity difference (Almirante–Punta Caracol). Data plotted are the near-bottom measurements for each high resolution profile (May 2015–March 2020). Color indicates time of year. For raw data: R = -0.42; p < 0.05.

hypothesis, the climatologies in Fig. 2 suggest that incoming water will thus have highest density, and therefore the highest potential for deep-water renewal, between January and June and again in September–November. These periods coincide with the normoxic period and the period of intermittent ventilation, respectively.

Although the lack of flow measurements prevents a comprehensive assessment of this ventilation model, a comparison of near-bottom salinity at Punta Caracol relative to Almirante shows a statistically significant relationship with the hypoxic state (Fig. 10). Although there is considerable scatter, there is evidence that when Almirante near-bottom water is saltier than Punta Caracol (to the right in Fig. 10), hypoxia tends to occur. In the context of the deep-water renewal model, Punta Caracol serves as a proxy for the water that will resupply the stagnant, near-bottom water mass in the back bay. Ventilation in the back bay occurs only when the salinity difference, which follows the seasonal cycle (as shown in color), is weak.

Although deep-water renewal as a mechanism for ventilation is typically observed in fjords, it is a process that can also apply to shallow tropical systems, like Bahía Almirante. Further work is needed to examine this model, including potential mixing mechanisms and locations. These mechanisms would be likely to be modulated by tidal and subtidal flows, variations in inflow layer thickness and by effects of stratification on mixing mechanics. The potential for bottom water ventilation is also likely to be affected by vertical mixing within the back bay and by radiative heating, both of which will reduce the barrier for deep-water renewal.

Co-occurrence of multiple stressors

Temperature inversions co-occur with low DO in bottom waters (Fig. 6c), suggesting that when stratification is high, conditions are favorable for development of both temperature inversions and low DO. Although increased temperature also reduces DO solubility, the observed temperature increases do not account for the magnitude of the DO reduction. The relationship between low DO and warmer bottom temperatures (Fig. 7) implies that the temperature inversions are, at least in part, a consequence of accumulated radiative heating of the bottom layer over time. Figure 2d shows that temperature inversions on the annual timescale are coincident with nearsurface water cooling; however, solar warming at depth, which has previously been shown to drive accelerated warming relative to the rest of a salinity-stratified water column (Wells et al. 2012), likely contributes to formation of the observed inversion in the temperature bay (Harrison Phizacklea 1987) because seasonal bottom temperatures increase (Fig. 2d). As such, temperature inversions and low-DO are consistent with long residence times, which allow for heat accumulation and DO depletion. The co-occurrence between temperature inversions and hypoxia indicates that benthic organisms may face multiple stressors simultaneously, which can have exacerbating effects. Temperatures exceeding an organism's thermal tolerance increase oxygen demand, and deoxygenated waters may reduce the optimal thermal range (Vaquer-Sunyer and Duarte 2011).

Summary

This study presents analysis of variability and seasonality of the hydrography and hypoxia for a tropical estuary system, Bahía Almirante, which experiences seasonal hypoxia at depth and frequent temperature inversions. The strongest, most persistent hypoxic events occur in the back bay, while the mid bay experiences intermittent hypoxia, and DO reductions at depth are common throughout the bay during the hypoxic period. Offshore DO values remain high, indicating that the sources of hypoxic waters do not originate from the open ocean. Temperature inversions exhibit a similar spatial pattern, with warmer temperatures at depth and stronger temperature inversions occurring in the back bay. They occur more frequently than hypoxia throughout the bay, including at the offshore site. Infrequent, relatively weak temperature inversions are also observed during the normoxic period. The common patterns in hypoxia and temperature inversions indicate that they are both related to the formation of an isolated deep layer in the bay. Seasonal averages suggest that strong vertical salinity stratification, which results from increased freshwater input, is a major contributing factor to the initiation of hypoxia. Hydrography indicates that the mechanisms that favor hypoxia are amplified in the back bay, where the strongest vertical stratification occurs.

The heat budget shows that there is net advective heat export from Bahía Almirante. The average residence time of 10-40 d likely does not represent the bay overall. For example, retention time is estimated to be longer in the back bay, consistent with the persistence of significant stratification and hypoxia in the back bay. We present evidence through a case study that lateral advection can play a critical role in hypoxia breakdown. The relationship between near bottom DO and bottom salinities in the mid bay and back bay is consistent with deep-water renewal as the mechanism for bottom water ventilation, as commonly observed in fjords. Our data show no statistical relationship between wind and stratification or wind and DO, however, the relative contribution of advection and wind-driven mixing as well as the contribution of other mechanisms for vertical mixing (including convective cooling and interfacial shear) remains an open question.

Bahía Almirante shares characteristics with other tropical estuaries, including seasonal patterns in surface heat flux and freshwater flux. The net heat export and prevalent temperature inversions are expected in other tropical coastal embayments. The high, weakly seasonal, precipitation impacts seasonal stratification and is expected to play a similarly important role in other shallow tropical systems. The posited mechanism for hypoxia breakdown, deep-water renewal, is not tropics-specific; however, it poses an interesting potential

mechanism for intermittent oxygen renewal in other tropical estuaries, and the governing processes require further study to be resolved.

The hypoxia and temperature inversions described above are of critical importance to the biological communities of Bahía Almirante. Although this study does not address organismal responses, it suggests that physical dynamics in Bahía Almirante contribute to conditions that are known to be stressors for marine organisms. Identifying mechanisms that govern hypoxia and temperature inversions provides the context needed to evaluate whether similar processes occur in other shallow, tropical estuaries, as well as how they compare to temperate coastal systems.

Data availability statement

posted online as part of the UC San Diego Library Digital Collections (doi: https://doi.org/10.6075/J0TT4R4K). Meteorological data sets are provided by the Physical Monitoring Program of the Smithsonian Tropical Research Institute (https://biogeodb.stri.si.edu/physical_monitoring/research/bocas). Publicly available satellite-based observations from NASA's Clouds and the Earth's Radiant Energy System (CERES) can be found at https://ceres.larc.nasa.gov/data/ and publicly available reanalysis wind and total precipitation data from The European Centre for Medium Range Weather Forecasts (ECMWF) can be found at https://cds.climate.copernicus.eu/cdsapp#!/dataset/reanalysis-era5-single-levels?tab=overview.

STRI Spatial sampling program and meteorological data are

References

- Altieri, A. H., S. B. Harrison, J. Seemann, R. Collin, R. J. Diaz, and N. Knowlton. 2017. Tropical dead zones and mass mortalities on coral reefs. Proc. Natl. Acad. Sci. **114**: 3660–3665. doi:10.1073/pnas.1621517114
- Altieri, A. H., M. D. Johnson, S. D. Swaminathan, H. R. Nelson, and K. B. Gedan. 2021. Resilience of tropical ecosystems to ocean deoxygenation. Trends Ecol. Evol. **36**: 227–238. doi:10.1016/j.tree.2020.11.003
- Andrade, C. A., and E. D. Barton. 2000. Eddy development and motion in the Caribbean Sea. J. Geophys. Res. Oceans **105**: 26191–26201. doi:10.1029/2000JC000300
- Avendaño-Alvarez, O., D. Salas-Monreal, M. Marin-Hernandez, D. A. Salas-de Leon, and M. A. Monreal-Gomez. 2017. Annual hydrological variation and hypoxic zone in a tropical coral reef system. Reg. Stud. Mar. Sci. **9**: 145–155. doi: 10.1016/j.rsma.2016.12.007
- Bates, N. R. 2017. Twenty years of marine carbon cycle observations at Devils Hole Bermuda provide insights into seasonal hypoxia, coral reef calcification, and ocean acidification. Front. Mar. Sci. **4**: 36.
- Boesch, D. F., and N. N. Rabalais. 1991. Effects of hypoxia on continental shelf benthos: Comparisons between the New York Bight and the Northern Gulf of Mexico. Geol. Soc.

- Lond. Spec. Publ. **58**: 27–34. doi:10.1144/GSL.SP.1991.058. 01.02
- Breitburg, D., and others. 2018. Declining oxygen in the global ocean and coastal waters. Science **359**: 7240. doi:10. 1126/science.aam7240
- Centurioni, L. R., and P. P. Niiler. 2003. On the surface currents of the Caribbean Sea. Geophys. Res. Lett. **30**: 1279. doi:10.1029/2002GL016231
- Chan, F., J. A. Barth, J. Lubchenco, A. Kirincich, H. Weeks, W. T. Peterson, and B. A. Menge. 2008. Emergence of anoxia in the California current large marine ecosystem. Science **319**: 920. doi:10.1126/science. 1149016
- Clark, K. E., and others. 2022. Land use and land cover shape river water quality at a Continental Caribbean land-ocean interface. Front. Water 4.
- Collin, R. 2005. Ecological monitoring and biodiversity surveys at the Smithsonian Tropical Research Institute s Bocas Del Toro Research Station. Caribbean J Sci. **41**: 367–373
- Collin, R., L. D'Croz, P. Gondola, and J. B. Del Rosario. 2009. Climate and hydrological factors affecting variation in chlorophyll concentration and water clarity in the Bahia Almirante, Panama. *In* Proceedings of the Smithsonian Marine Science Symposium. Smithsonian Institution Scholarly Press.
- Corredor, J. E., R. W. Howarth, R. R. Twilley, and J. M. Morell. 1999. Nitrogen cycling and anthropogenic impact in the tropical interamerican seas, p. 163–178. *In* New perspectives on nitrogen cycling in the temperate and tropical Americas. Springer.
- Cramer, K. L. 2013. History of human occupation and environmental change in western and Central Caribbean Panama. Bull. Mar. Sci. **89**: 955–982. doi:10.5343/bms. 2012.1028
- D'Croz, L., J. B. del Rosario, and P. Gondola. 2005. The effect of fresh water runoff on the distribution of dissolved inorganic nutrients and plankton in the Bocas del Toro archipelago, Caribbean Panama. Caribb. J. Sci. **41**: 414–429
- Diaz, R. J., and R. Rosenberg. 2008. Spreading dead zones and consequences for marine ecosystems. Science **321**: 926–929. doi:10.1126/science.1156401
- Fairall, C. W., E. F. Bradley, D. P. Rogers, J. B. Edson, and G. S. Young. 1996. Bulk parameterization of air-sea fluxes for tropical ocean-global atmosphere coupled-ocean atmosphere response experiment. J. Geophys. Res. Oceans **101**: 3747–3764. doi:10.1029/95JC03205
- Farmer, D. M., and H. J. Freeland. 1983. The physical oceanography of fjords. Prog. Oceanogr. **12**: 147–219. doi:10.1016/0079-6611(83)90004-6
- Fennel, K., and J. M. Testa. 2019. Biogeochemical controls on coastal hypoxia. Ann. Rev. Mar. Sci. **11**: 105–130. doi:10. 1146/annurev-marine-010318-095138
- Gade, H. G., and A. Edwards. 1980. Deep water renewal in fjords, p. 453–489. *In* Fjord oceanography. Springer.

- Gallegos, A. 1996. Descriptive physical oceanography of the Caribbean Sea. American Geophysical Union (AGU). Chap. 3, p. 36–55.
- Gilbert, D., N. N. Rabalais, R. J. Diaz, and J. Zhang. 2010. Evidence for greater oxygen decline rates in the coastal ocean than in the open ocean. Biogeosciences **7**: 2283–2296. doi: 10.5194/bg-7-2283-2010
- Goreau, T. J., and R. L. Hayes. 1994. Coral bleaching and ocean "hot spots". Ambio J. Hum. Environ. Res. Manage. **23**: 176–180.
- Harrison, S. J., and A. P. Phizacklea. 1987. Vertical temperature gradients in muddy intertidal sediments in the Forth estuary, Scotland 1. Limnol. Oceanogr. **32**: 954–963. doi:10. 4319/lo.1987.32.4.0954
- Howarth, R. W. 2008. Coastal nitrogen pollution: A review of sources and trends globally and regionally. Harmful Algae **8**: 14–20. doi:10.1016/j.hal.2008.08.015
- Hughes, D. J., R. Alderdice, C. Cooney, M. Kühl, M. Pernice, C. R. Voolstra, and D. J. Suggett. 2020. Coral reef survival under accelerating ocean deoxygenation. Nat. Clim. Change **10**: 296–307. doi:10.1038/s41558-020-0737-9
- Johnson, M. D., L. M. Rodriguez, and A. H. Altieri. 2018. Shallow-water hypoxia and mass mortality on a Caribbean coral reef. Bull. Mar. Sci. 94: 143–144. doi:10.5343/bms.2017.1163
- Kaufmann, K., and R. C. Thompson. 2005. Water temperature variation and the meteorological and hydrographic environment of Bocas del Toro, Panama. Caribb. J. Sci. **41**: 392–413
- Kealoha, A. K., S. M. Doyle, K. E. F. Shamberger, J. B. Sylvan, R. D. Hetland, and S. F. DiMarco. 2020. Localized hypoxia may have caused coral reef mortality at the Flower Garden Banks. Coral Reefs 39: 119–132. doi:10.1007/s00338-019-01883-9
- Kemp, W. M., J. M. Testa, D. J. Conley, D. Gilbert, and J. D. Hagy. 2009. Temporal responses of coastal hypoxia to nutrient loading and physical controls. Biogeosciences **6**: 2985–3008. doi:10.5194/bg-6-2985-2009
- Levin, L. A., and D. L. Breitburg. 2015. Linking coasts and seas to address ocean deoxygenation. Nat. Clim. Change **5**: 401–403. doi:10.1038/nclimate2595
- Li, A., and M. A. Reidenbach. 2014. Forecasting decadal changes in sea surface temperatures and coral bleaching within a Caribbean coral reef. Coral Reefs **33**: 847–861. doi: 10.1007/s00338-014-1162-1
- Lucey, N., E. Haskett, and R. Collin. 2020. Multi-stressor extremes found on a tropical coral reef impair performance. Front. Mar. Sci. **7**: 1079.
- MacDonald, D. G., and W. R. Geyer. 2004. Turbulent energy production and entrainment at a highly stratified estuarine front. J. Geophys. Res. Oceans **109**: C05004. doi:10.1029/2003JC002094
- McDougall, T. J., and P. M. Barker. 2011. Getting started with TEOS-10 and the Gibbs Seawater (GSW) oceanographic toolbox. SCOR/IAPSO WG, v. **127**. p. 1–28.

- NASA/LARC/SD/ASDC. 2015. CERES regionally averaged TOA fluxes, clouds and aerosols hourly Terra Edition4A. NASA Langley Atmospheric Science Data Center DAAC.
- Neal, B. P., C. Condit, G. Liu, S. dos Santos, M. Kahru, B. G. Mitchell, and D. I. Kline. 2014. When depth is no refuge: Cumulative thermal stress increases with depth in Bocas del Toro, Panama. Coral Reefs 33: 193–205. doi:10.1007/s00338-013-1081-6
- Nittrouer, C. A., G. J. Brunskill, and A. G. Figueiredo. 1995. Importance of tropical coastal environments. Geo-Mar. Lett. **15**: 121–126.
- Paton, S. 2020. Data sets provided by the physical monitoring program of the Smithsonian Tropical Research Institute. Smithsonian Tropical Research Institute.
- Pawlowicz, R., B. Beardsley, S. Lentz, E. Dever, and A. Anis. 2001. Wiley Online Library. Software simplifies air-sea data estimates. doi:10.1029/01EO00004
- Payne, R. E. 1972. Albedo of the sea surface. J Atmos Sci **29**: 959–970. doi:10.1175/1520-0469(1972)029<0959:AOTSS> 2.0.CO:2
- Pomeroy, L. R., and W. J. Wiebe. 2001. Temperature and substrates as interactive limiting factors for marine heterotrophic bacteria. Aquat. Microb. Ecol. 23: 187–204.
- Rabalais, N. N., R. J. Diaz, L. A. Levin, R. E. Turner, D. Gilbert, and J. Zhang. 2010. Dynamics and distribution of natural and human-caused hypoxia. Biogeosciences **7**: 585–619. doi:10.5194/bg-7-585-2010
- Salamena, G. G., J. C. Whinney, S. F. Heron, and P. V. Ridd. 2021. Internal tidal waves and deep-water renewal in a tropical fjord: Lessons from Ambon Bay, eastern Indonesia. Estuar. Coast. Shelf Sci. **253**: 107291. doi:10.1016/j.ecss. 2021.107291
- Scranton, M. I., and others. 2014. Interannual and subdecadal variability in the nutrient geochemistry of the Cariaco Basin. Oceanography **27**: 148–159. doi:10.5670/oceanog. 2014.18
- Scully, M. E. 2013. Physical controls on hypoxia in Chesapeake Bay: A numerical modeling study. J. Geophys. Res. Oceans **118**: 1239–1256. doi:10.1002/jgrc.20138
- Silva, N., and C. A. Vargas. 2014. Hypoxia in Chilean patagonian fjords. Prog. Oceanogr. **129**: 62–74. doi:10.1016/j. pocean.2014.05.016
- Smith, R. 1976. Longitudinal dispersion of a buoyant contaminant in a shallow channel. J. Fluid Mech. **78**: 677–688.
- Stanley, D. W., and S. W. Nixon. 1992. Stratification and bottom-water hypoxia in the Pamlico River estuary. Estuaries **15**: 270–281. doi:10.2307/1352775
- Talley, L. D. 2011. Descriptive physical oceanography: An introduction. Academic Press.
- Vaquer-Sunyer, R., and C. M. Duarte. 2008. Thresholds of hypoxia for marine biodiversity. Proc. Natl. Acad. Sci. **105**: 15452–15457. doi:10.1073/pnas.0803833105
- Vaquer-Sunyer, R., and C. M. Duarte. 2011. Temperature effects on oxygen thresholds for hypoxia in marine benthic

Seasonal hypoxia in a tropical bay

- organisms. Glob. Chang. Biol. **17**: 1788–1797. doi:10.1111/j.1365-2486.2010.02343.x
- Vieillard, A. M., S. E. Newell, and S. F. Thrush. 2020. Recovering from bias: A call for further study of underrepresented tropical and low-nutrient estuaries. J. Geophys. Res. Biogeosci. **125**: e2020JG005766. doi:10.1029/2020JG005766
- Wells, J. R., J. P. Fram, and G. Pawlak. 2012. Solar warming of near-bottom water over a fringing reef. J. Mar. Res. **70**: 641–660. doi:10.1357/002224012805262734
- Wetz, M. S., B. Hales, Z. Chase, P. A. Wheeler, and M. M. Whitney. 2006. Riverine input of macronutrients, iron, and organic matter to the coastal ocean off Oregon, USA, during the winter. Limnol. Oceanogr. **51**: 2221–2231. doi:10. 4319/lo.2006.51.5.2221
- Wiseman, W. J., N. N. Rabalais, R. E. Turner, S. P. Dinnel, and A. N. D. A. MacNaughton. 1997. Seasonal and interannual variability within the Louisiana coastal current: Stratification and hypoxia. J. Mar. Syst. **12**: 237–248.

Acknowledgments

The authors would like to thank Plinio Gondola and the environmental monitoring staff at STRI's Bocas del Toro Research Station and volunteers who have collected the long-term data set. The authors would also like to thank Steve Patton for the maintenance of the meteorological data. All data have been collected under permits from MiAmbiente and ARAP. A.E.A. was supported by a Smithsonian Fellowship. This work was supported by a National Science Foundation grant, NSF OCE—1924220 (R.C.), NSF OCE—1924551 (G.P.), NSF OCE—1924664 (K.A.D.).

Conflict of Interest

None declared.

Submitted 03 November 2021 Revised 29 April 2022 Accepted 20 June 2022

Associate editor: Maitane Olabarrieta